Available free online at www.medjchem.com

Mediterranean Journal of Chemistry

Mediterranean Journal of Chemistry **2020**, 10(1), 33-45

Adsorption Study of Malachite Green Removal from Aqueous Solution Using Cu/M^{3+} (M^{3+}=Al, Cr) Layered Double Hydroxide

Neza Rahayu Palapa [1], Risfidian Mohadi [1, 2], Addy Rachmat [1, 2] and Aldes Lesbani [1, 2, *]

[1] Graduate School of Science, Faculty of Mathematics and Natural Sciences, Universitas Sriwijaya, Jl. Palembang-Prabumulih, Km. 32, Ogan Ilir, South Sumatra, Indonesia

[2] Research Centre of Inorganic Materials and Coordination Complexes, Faculty of Mathematics and Natural Sciences, Universitas Sriwijaya

Abstract: Layered double hydroxide (LDH) Cu/Al and Cu/Cr had been used as adsorbent of malachite green (MG) in aqueous solution. The properties of Cu/Al and Cu/Cr LDHs were analyzed by X-ray diffraction, surface area analysis (BET) and FTIR spectroscopy. Adsorption study of MG was achieved at pH 9. Adsorption of MG follows the pseudo-second-order kinetic model. Langmuir isotherm was suitable for adsorption of MG on both LDH with a maximum adsorption capacity of 59.52 mg/g. The thermodynamic study indicated that the adsorption process is physisorption, spontaneous, and endothermic process. Adsorption of MG onto LDHs involve the acid-base interaction between adsorbent and adsorbate.

Keywords: Layered double hydroxide, malachite green, adsorption, kinetic, thermodynamic.

1. Introduction

The use of reactive dye in the textile industry for ethnic fabric and clothes increases sharply in this decade. The textile industry contributes a significant number of liquid effluent pollutants [1], due to the high quantities of dyes and water used in the coloring processes [2]. Textile wastewater is a complex mixture and contains a highly polluting substance, i.e., heavy metal cations, and dye [3]. Most of dyes substance contained aromatic structure, which makes them toxic [4], non-biodegradable, and also carcinogenic for humans and the environment [5,6]. In the environment, these colored effluent's was covering the surface of waters and reduced the oxygen [7]. In order to remove pollutants in wastewater, several techniques have been developed, such as adsorption [8], filtration [9], coagulation [10] and photocatalysis [11]. Among these methods, adsorption is a suitable method to remove dye from the aqueous solution because it is an easy technique, fast, cheap, and has no pollutants [12,13]. The adsorption of several dyes has been reported by using various sorbents, i.e. activated carbon [14], algae [15], alumina-MOF [16], sawdust modification [17,18], kaolin [5], bentonite [19,20] and layered double hydroxide [21,22].

Layered double hydroxide was studied as sorbent because of their adsorption ability due to exchangeable anion in the interlayer, high surface area and accessible to synthesized [23–25]. Recently, layered double hydroxide was used as a sorbent of dyes such as Ca/Al after being modified through the solvothermal method. The modified LDH applied for adsorption congo red and showed adsorption capacity 228 mg/g [26]. Mg/Al-NO_3 LDH was reported in adsorption of methyl orange with adsorption capacity 144 mg/g [27]. Mg/Al LDH also reported in adsorption of methylene blue with adsorption capacity 80 mg/g [28] whereas Ni/Fe LDH was reported in adsorption of methyl orange having adsorption capacity 205 mg/g [29]. Layered double hydroxide, also known as hydrotalcite, has cations substituted by other divalent and a trivalent metal cation. The general formula of layered double hydroxide is $[M_{1-x}^{2+}M_x^{3+}(OH)_2]^{x+}A_{x/n}^{n-}\cdot mH_2O$, with A^n as exchangeable anion interlayer [30–33]. Various methods of synthesis of layered double hydroxide by using a different combination of cations were reported such as co-precipitation [34], sol-gel [35], hydrothermal [36] and hydrolysis [37]. The mixed metal salts solutions dissolved followed by aging with hydrothermal treatment [33] or without high temperature for more extended times [23].

In present work, Cu/Al and Cu/Cr layered double hydroxide was synthesis by co-precipitation method. The physicochemical of sorbent were characterized by X-ray diffraction, surface area analysis carried out by adsorption-desorption N_2 BET method and the functional groups evaluated using FTIR.
The malachite green dye is selected as a model pollutant in this study. Adsorption study also was

*Corresponding author: Aldes Lesbani
Email address: aldeslesbani@pps.unsri.ac.id
DOI: http://dx.doi.org/10.13171/mjc10102001261236al

Received December 12, 2019
Accepted January 2, 2020
Published January 27, 2020

aimed to determine kinetic and isotherm adsorption parameters models by varying adsorption times, dyes initial concentration, pH, and temperature of adsorption. The desorption study was examined in several solvents to determine the optimum conditions for the desorption of MG.

2. Experimental

2.1. Materials and Instrumentation

All chemical reagents was purchased by Merck and Sigma Aldrich such as copper nitrate $Cu(NO_3)_2.6H_2O$, aluminum nitrate $Al(NO_3)_3.9H_2O$, chromium nitrate $Cr(NO_3)_3.9H_2O$, sodium hydroxide NaOH, sodium carbonate Na_2CO_3, chloride acid HCl and malachite green (4-{[4-(Dimethylamino) phenyl](phenyl)methylidene}-N,N-dimethylcyclo-hexa-2,5-dien-1-iminium chloride). Water was obtained by Purite® water purification at Universitas Sriwijaya. XRD Rigaku Miniflex-600 conducted the characterization of sorbents, and the sample scanned at scan speed 1 deg.min^{-1}. Surface area analyses were conducted using BET ASAP Micromeritics 2020 at 77 K. Infrared was conducted using FTIR Shimadzu Prestige- 21 by KBr disc and was scanned at wavenumber 300-4000 cm^{-1}. The concentration of dye was analyzed using UV-Visible spectro-photometer BK-UV1800 at wavelength 619 nm.

2.2. Methods

Synthesis of Cu/Al and Cu/Cr LDHs [38]

The synthesis of Cu/Al-LDH carried out by adding 0.75 M copper nitrate solution into 0.25 M aluminum nitrate followed by vigorous stirring for an hour. In a separate glass, 2 M sodium hydroxide added simultaneously into 1 M sodium carbonate, and then after an hour, added drop wisely at room temperature with vigorous stirring for six hours. The pH was adjusted at 10 by adding aqueous NaOH. After six hours, the mixing solution aged at 80ºC overnight. The Cu/Al-LDH was washed and dried in room temperature to obtained Cu/Al LDH. The synthesis of Cu/Cr-LDH was carried out in a similar way to Cu/Al-LDH. The divalent and trivalent metal cation ratio was unchanged. 0.75 M of copper nitrate and 0.25 M of chromium nitrate.

3. Results and Discussion

3.1. Adsorbent Characterization

Cu/Al and Cu/Cr-LDHs were successfully synthesized by co-precipitation method using the mixture of a metal cation and base solution (Na_2CO_3 and NaOH). The molar ratio adjusted to 3:1 and the pH mixture solution were setup around 9-10 at 80ºC. After precipitation solidly aged for overnight, the mixture gel was dried at room temperature. According to Bukhtiyarova (2019), the pure LDH was obtained by kept pH 10-11 as long as the synthesis process [23]. The Powder X-ray diffraction results are shown in Fig.1. Cu/Al and Cu/Cr-LDHs have a similar pattern, which represented the formation of well-ordered layered materials. The characteristic pattern of LDH indicated by (003), (006), (012), (110) and (113) reflections.

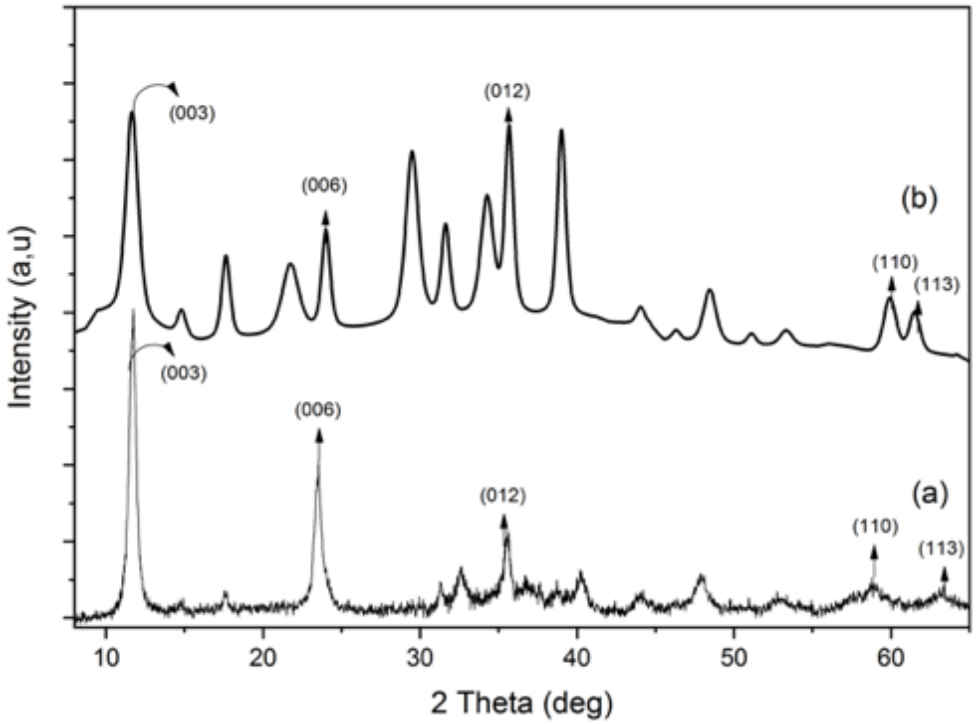

Figure 1. X-ray powder diffraction of Cu/Al-LDH (a) and Cu/Cr-LDH (b)

The d-spacing value (003) by Bragg's equation was calculated 0.754 nm from 2θ value at 11.7° for Cu/Al-LDH and 0.758 nm Å from 2θ value at 11.6° for Cu/Cr-LDH. Powder XRD pattern of Cu/Cr sample shows the noise peaks at 30 °, which indicate the crystal impurities (the presences of $Na[Al(OH)_4]$). This impurity usually formed because of high concentration of NaOH, which reacted with aluminum at high pH. Another impurity shows by 2θ value at 34° indicates the presence of copper oxide.

The diffraction pattern of Cu/Al and Cu/Cr-LDH diffractions represent a rhombohedral structure and a 3R polytypism of LDH. according to Zhitova the unit-cell parameters were determined as follows: 'a' = 2d(110) and 'c' = 3d(003) [39]. The calculated lattice parameters are shown in Table 1. The values of 'c' parameter of both LDH are similar because of the presence of nitrate anion in the interlayer. The difference in the 'a' parameter caused by the difference in ionic radii of lower Al^{3+} (0.50 Å) compared to Cr^{3+} (0.61 Å).

Table 1. Lattice parameters and BET surface area of both LDH samples.

LDH	Lattice Parameters (nm)			Pore Volume	BET Surface	Pore Size
	d(003)	a	c	cm^3/g	m^2/g	nm
Cu/Al	0.754	0.31	2.262	0.116	46.2	10.39
Cu/Cr	0.758	0.31	2.274	0.015	4.67	14.39

The nitrogen adsorption-desorption isotherms of Cu/Al and Cu/Cr-LDHs showed in Fig.2. The curve of adsorption-desorption indicates type IV, which belongs to mesoporous materials. The hysteresis loop of these materials is H3-type, which consistent with cavitation-induced evaporation, which is the cavitation threshold, is exceeded hysteresis loop (*P/Po*) > 0.42. The H3 hysteresis explained that the binding strength of anion located in the interlayer. Table 1 shows the BET surface areas, pore volume and pore size of Cu/Al and Cu/Cr-LDH. According to IUPAC classification, the pore size of both LDH is a mesopore type. The calculated BET surface areas for Cu/Al-LDH (46.2 m^2/g) shows that it is tenfold bigger compared to Cu/Cr-LDH (4.67 m^2/g).

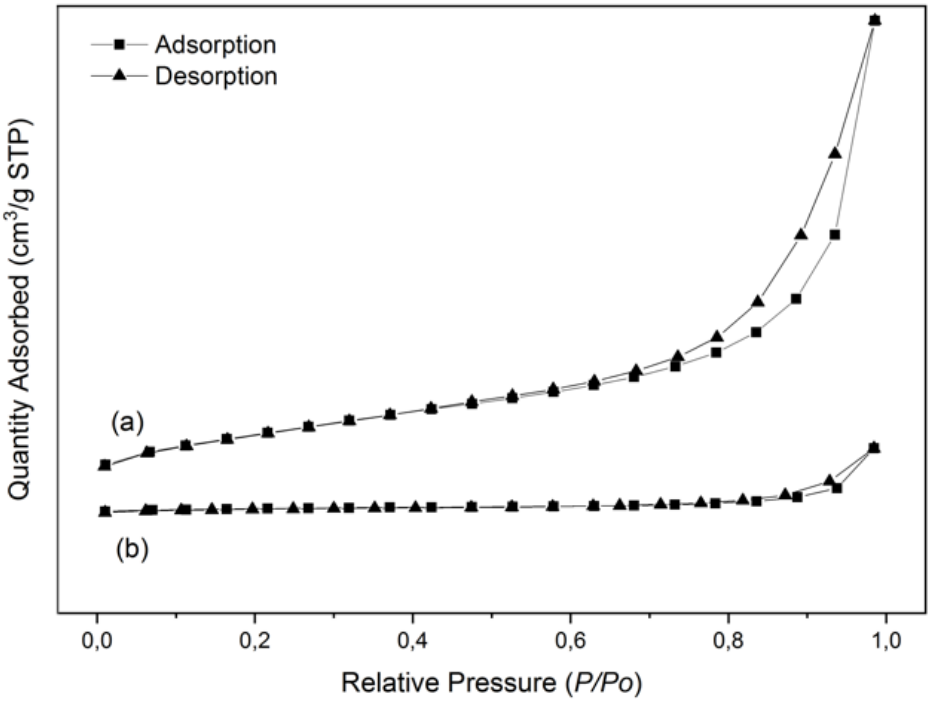

Figure 2. Adsorption-desorption N_2 profile of Cu/Al LDH (a) and Cu/Cr LDH (b)

The FTIR spectra of the Cu/Al and Cu/Cr-LDH are shown in Fig.3. The broad vibration of hydroxyl groups (O-H stretching) in brucite layers and interlayer was confirmed at 3420 cm^{-1} for both of LDH. The lower vibration at 1635 cm^{-1} belongs to O-H bending. Cu/Al and Cu/Cr-LDHs both have nitrate anion in the interlayer. The anion confirmed by the intense peak in Fig.3 and was denoted as NO_3^- vibration for both LDH. The metal-oxide vibrations (Cu-O and Cr-O) are shown at 455 cm^{-1} and 568 cm^{-1}. Fig.3b represents the FTIR spectra of Cu/Al-LDH. Cu/Al-LDH has M-O vibrations at 455 cm^{-1} and 833 cm^{-1} which is assigned for Cu-O and Al-O vibration, respectively.

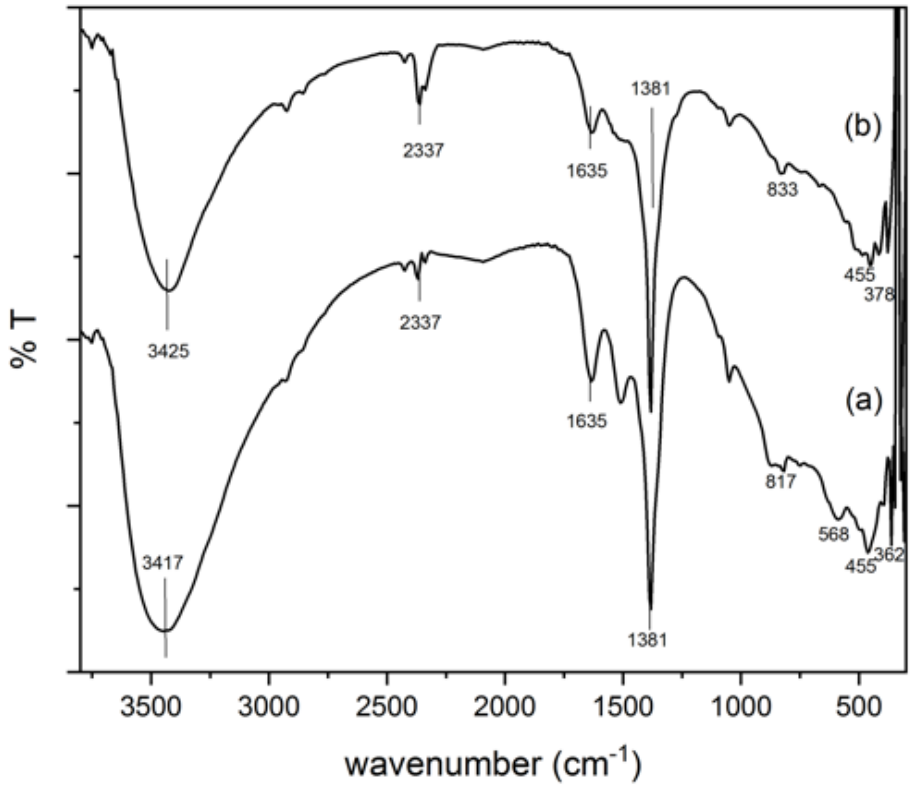

Figure 3. FTIR spectra of Cu/Cr-LDH (a) and Cu/Al-LDH (b)

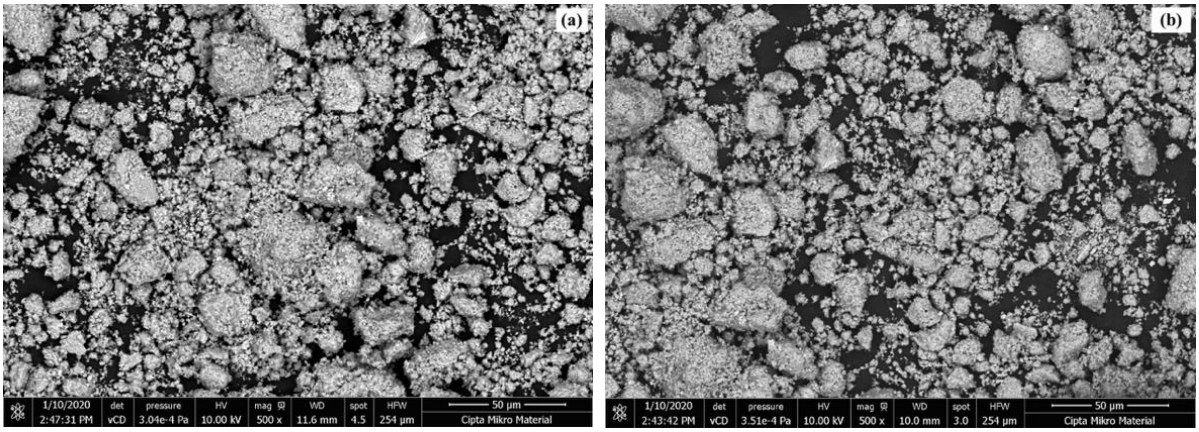

Figure 4. SEM images of Cu/Al LDH (a) and Cu/Cr-LDH (b)

The morphology of Cu/Al and Cu/Cr LDH was investigated by SEM Quanta-650 OXFORD Instrument and the result is shown on Fig.4. The morphology of Cu/Al and Cu/Cr LDH present the heterogeneity with round shape and aggregated particles on the surface. The similar result reported by Mao et al. 2018, the aggregated morphologies caused by high temperature during synthesis [40]. According to Bukhtiyarova 2019; Parida and Mohapatra 2012, LDHs has morphology "sand Rose" which is irregular layer shape with agglomerated particles in the surface of materials [23,41].

3.2. Effect of pH on Adsorption Malachite Green by Cu/Al and Cu/Cr LDH

The adsorption process was conducted by mixing LDHs with MG solution in various pH condition to obtain maximum removal of MG. The pH condition of adsorption was adjusted within range 4-11 (Fig.5). The optimum pH obtained at pH 9 and then decreases at 10-11. The MG removal achieves at 21.471 % and 20.473 % from 50 mg/L initial solution, respectively. The result is by what had been reported by Das et al. (2018). This author was using Mg/(Al+Fe) Ternary LDH to remove MG from its aqueous solution [42]. The increasing amount of adsorption occurs due to the change of active sites of the LDH, which is rich in OH^- and accumulated on the LDH surface to form negatively charged. At a higher pH, the surface site was deprotonated, and through the electrostatic bond, interaction occurs between the surface site and cationic dye molecules.

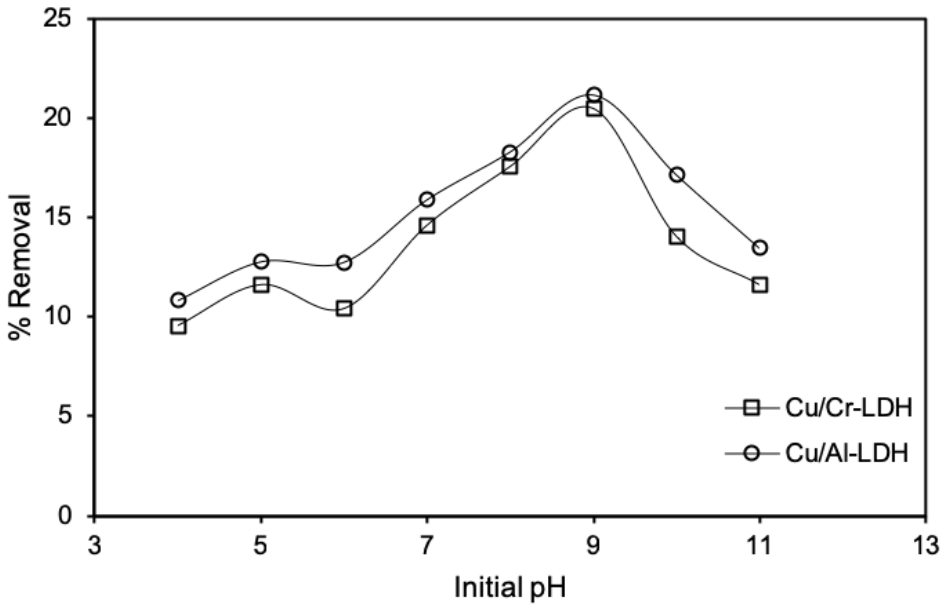

Figure 5. pH effect dye solution of adsorption malachite green by Cu/Al-LDH and Cu/Cr-LDH

The maximum wavelength (λ_{max}) of selected dyes measured in two different pH condition (4 and 9) by UV-Vis spectrophotometer at 400-800 nm is displayed on Fig.6. The adsorption selectivity of LDHs against selected dyes can be traced from changes of λ_{max} measurement during adsorption time. The dyes mixture comprised of malachite green (MG), methylene blue (MB) and rhodamine-B (RhB). The UV-Visible spectra shown in Fig.6. In both conditions of acid and base, λ_{max} remains unchanged for all dyes. The adsorption selectivity of LDH for cationic dyes removal best condition is at pH 9 as indicated by well-separated peaks. Fig.6a and 6d show that for Cu/Al and Cu/Cr LDH has efficiency remove MG in base condition at 10 ppm but not significant at 25 ppm (Fig.6b and 6e). Among the cationic dyes, MG was being adsorbed more then methylene blue (MB) and rhodamine-B (RhB) at the base condition. The decreases in absorbance line with a contact time of adsorption confirm that sorbent-adsorbate interactions will continue to occur at pH 9 until the condition of equilibrium reached. In acid conditions (pH 4), the cationic dyes mixture does not interact in both LDHs. Low pH affected the LDH surface and turned it into positively charged and repels cationic dye molecules.

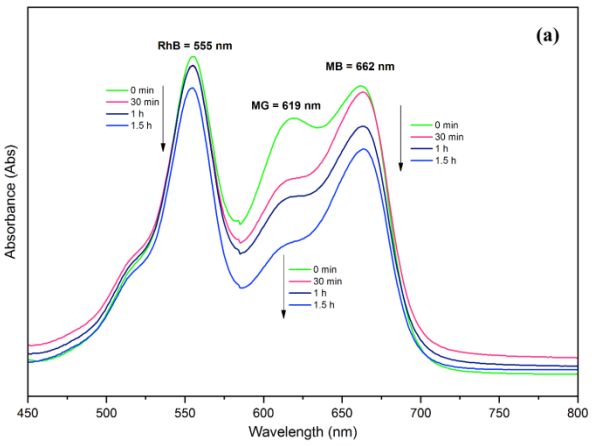

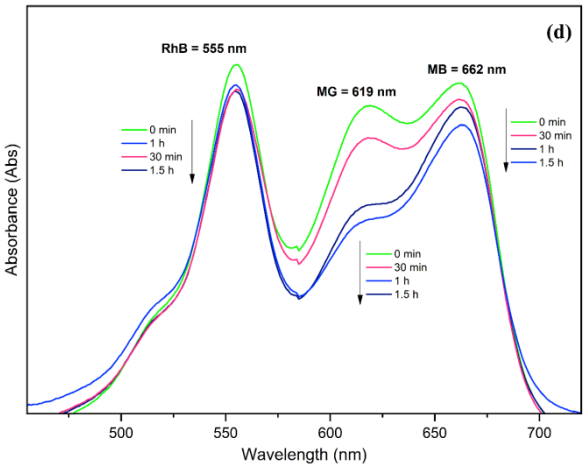

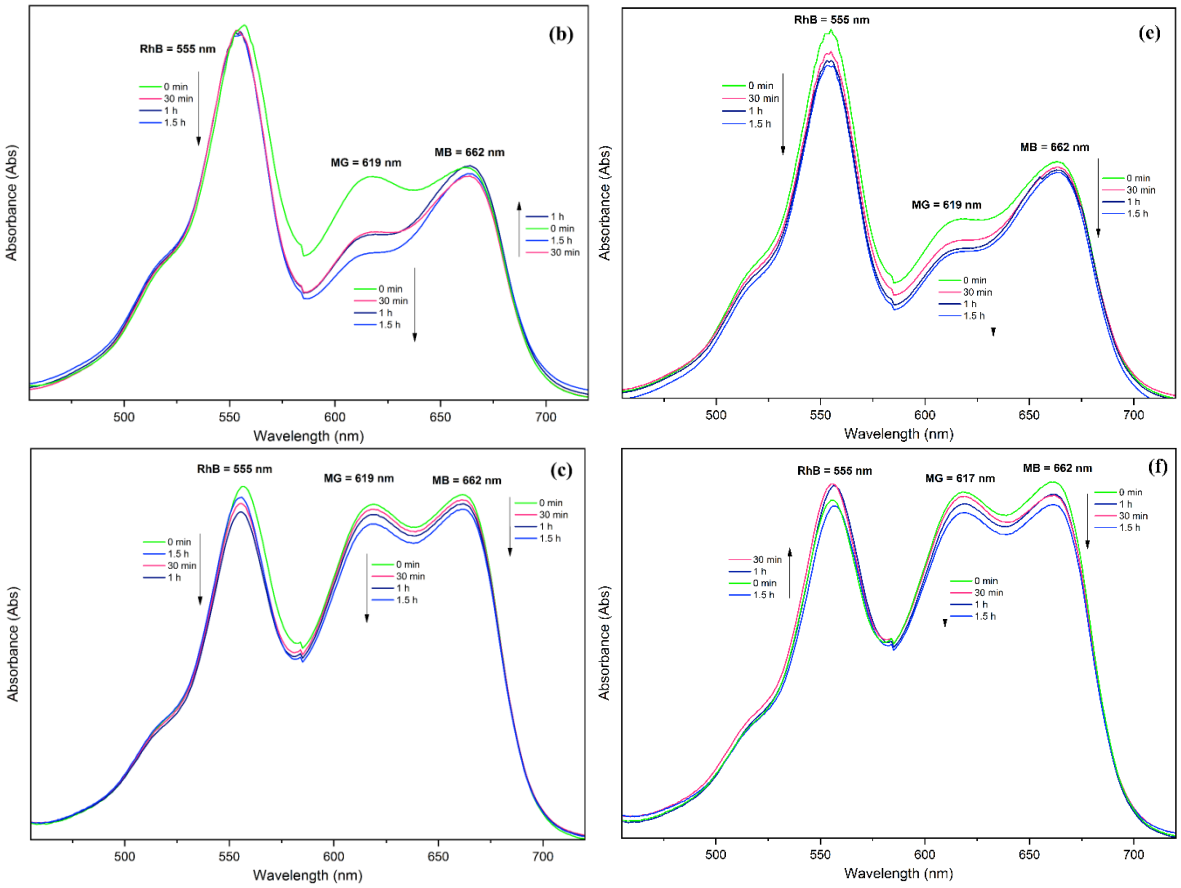

Figure 6. UV-Visible spectra of mixture cationic dyes (MB, MG and RhB) with (a) 10 ppm pH 9 by CuAl, (b) 25 ppm pH 9 by CuAl, (c) 10 ppm pH 4 by CuAl, (d) 10 ppm pH 9 by CuCr, (e) 25 ppm pH 9 by CuCr and (f) 10 ppm pH 4 by CuCr (sorption process in several times)

3.3. Effect of contact time

For several initial concentrations, the contact time was adjusting for determining the relationship between MG removal to contact time. The adsorption condition was adjusted at pH 9 (50 mg and 50 mL MG solution in several concentrations). Fig.7 shows that the dye uptake increased rapidly with time and after that reach equilibrium.

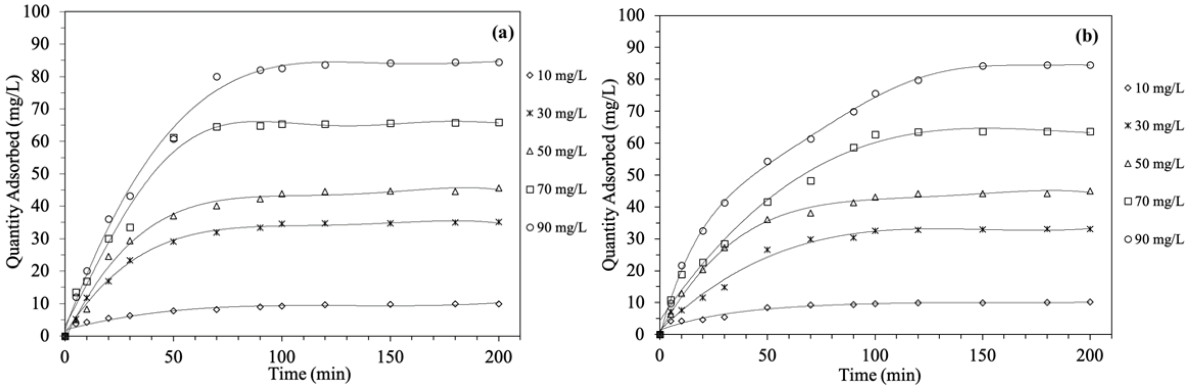

Figure 7. Malachite green uptake by varying times in several concentrations of Cu/Al-LDH (a) and Cu/Cr-LDH

For Cu/Al-LDH (Fig.7a), the equilibrium was reached at 50 min for 10-50 mg/L, but for MG solution with a higher concentration (70-90 mg/L), the equilibrium was reached at 70 min. Furthermore, the increase of adsorption capacity was caused by the driving force of the concentration gradient from increases initial concentration. Fig.7b shows the effect of time from MG removal by Cu/Cr-LDH in several initial concentrations. The equilibrium was reached at 50 min for lower concentration and higher concentration at 120 min. Fig.7b was shown too that an increasing initial concentration of MG causes the increase the MG removal uptake.

Adsorption kinetics was studied by pseudo-first-order and pseudo-second-order to predicted the mechanism

process of Cu/Al and Cu/Cr-LDH sorption. The pseudo-first-order (PFO) equation was followed:

$$\log(qe - qt) = \log qe - \frac{k_1 t}{2.303} \quad (1)$$

Moreover, pseudo-second-order (PSO) can be expressed to:

$$\frac{t}{qt} = \frac{1}{k_2\, qe^2} + \frac{1}{qe} t \quad (2)$$

With q_e denotes adsorption capacity at equilibrium, k_1 is the rate constant of PFO, k_2 is the rate constant for PSO. The rate constant was obtained from plotting the equation to get correlation coefficients and listed in Table 2.

The parameters and correlation coefficients (R^2) obtained from linear plotting log(qe-qt) vs t (PFO) and t/qt vs t (PSO) was listed in Table 2. The result showed based on R^2, Cu/Al and Cu/Cr-LDH were >0.977 for PSO then PFO. This also supported by the $qe_{(calc)}$ PSO was close to the $qe_{(experiment)}$. This phenom indicated that the adsorption was following PSO kinetic model, which represents that electrostatic attraction from sorbent-sorbate. Additionally, the decreasing k_2 values over the increasing MG initial concentrations reflected in the shorter time needed by the respective systems to achieve equilibrium at lower initial concentrations [43]. In other words, the higher the k_2 value indicates, the adsorbate molecule is reactive condition.

Table 2. Kinetic parameters of Cu/Al and Cu/Cr-LDH

			PFO			PSO		
LDH	Co (mg/L)	$q_{e\,(exp)}$	$q_{e(calc)}$ (mg/g)	k_1 (min^{-1})	R^2	$q_{e(calc)}$ (mg/g)	k_2 (gmg/min)	R^2
Cu/Al	10	6.206	5.076	0.024	0.990	6.562	0.0116	0.993
	30	21.918	20.123	0.033	0.980	24.393	0.0021	0.987
	50	28.532	21.679	0.023	0.924	32.887	0.0015	0.963
	70	41.166	38.691	0.042	0.971	46.418	0.0010	0.977
	90	52.797	61.507	0.043	0.980	72.651	0.0006	0.983
Cu/Cr	10	6.339	5.119	0.027	0.983	6.813	0.0090	0.988
	30	20.655	24.063	0.041	0.977	28.218	0.0014	0.984
	50	28.116	23.471	0.025	0.948	31.518	0.0010	0.986
	70	39.799	47.285	0.040	0.937	64.441	0.0006	0.985
	90	52.789	65.002	0.038	0.924	70.627	0.0001	0.982

3.4. Effect of temperature and isotherm modeling

The effect of increasing temperature in several concentrations has affected increasing dye uptake for Cu/Al and Cu/Cr-LDH. The effect of temperature was investigated over the temperature range 303-323 K. Fig.8 represents the MG uptake in several concentrations for Cu/Al-LDH. The higher MG removal was shown at 323 K amount of 27.80 mg/g in higher concentration (100 mg/L). Fig.8b shows the higher MG uptake at 323 K amount 25.217 mg/g. According to Das (2018), the increasing dye uptake while increases temperature caused the decreases solution's viscosity, increase porosity or interlayer, resulting in the enhancement of active sites form adsorbent [40].

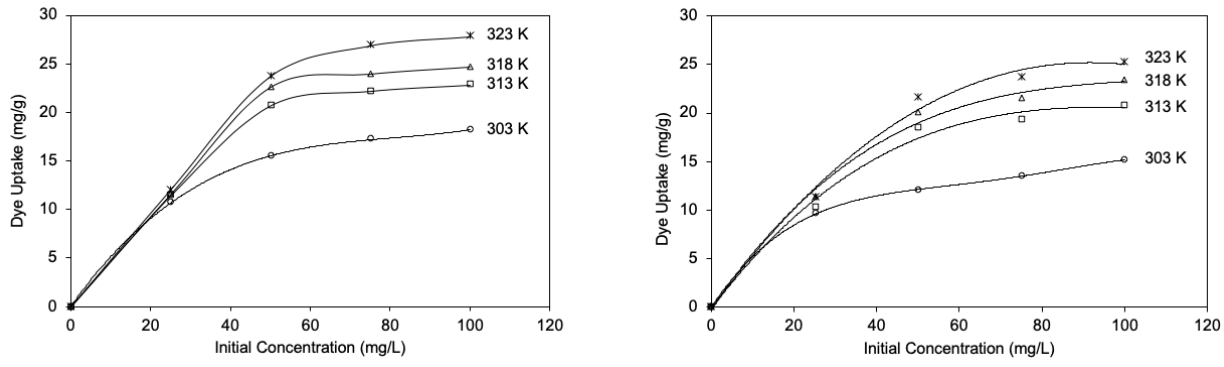

(a) (b)

Figure 8. Malachite green uptake by initial concentration in several temperatures of Cu/Al-LDH (a) and Cu/Cr-LDH (b)

Adsorption isotherm was studied using Freundlich and Langmuir model to analyzed the adsorption process. The Freundlich isotherm adsorption model has usually described multilayer process in heterogeneous surface, and the Langmuir isotherm is also popular to describe interact of adsorbent-adsorbate which extent in one layer or one site

occupied in the homogeneous surface. The linear form of Langmuir isotherm follows:

$$\frac{Ce}{qe} = \frac{1}{q_{max}} C_e + \frac{1}{q_{max} k_L} \quad (3)$$

Freundlich isotherm model is given as:

$$\text{Ln } q_e = \ln k_F + \frac{1}{n} \ln C_e \quad (4)$$

Where, q_{max} and k_L are Langmuir constants, k_F and n are Freundlich constants with n giving an indication of favorable the adsorption process and verify the type of adsorption process. The isotherm adsorption parameters were shown in Table 3. The result indicated that R^2 for Langmuir than Freundlich means that the adsorption of MG by Cu/Al and Cu/Cr-LDH are monolayer adsorption. In Table 3. Cu/Al-LDH has maximum adsorption capacity are 42.31; 51.04; 53.68 and 59.523 mg/g. Cu/Cr-LDH has maximum adsorption capacity are 41.119; 48.993; 51.524 and 55.865 mg/g in several temperatures. This value is in the better than adsorption capacity of other sorbents was previously reported, as shown in Table 4.

Table 3. Isotherm adsorption parameters of Cu/Al and Cu/Cr LDHs.

			T (K)			
LDH	Adsorption Isotherm	Adsorption Constant	303	313	318	323
Cu/Al	Langmuir	Q_{max}	42.31	51.04	53.68	59.523
		k_L	0.2191	0.314	0.44	0.2807
		R^2	0.9815	0.997	0.996	0.998
	Freundlich	n	3.35	4.056	3.47	4.87
		k_F	7.812	19.611	17.67	28.86
		R^2	0.9099	0.980	0.990	0.984
Cu/Cr	Langmuir	Q_{max}	41.119	48.993	51.524	55.865
		k_L	0.403	0.073	0.36	0.38
		R^2	0.999	0.990	0.997	0.999
	Freundlich	n	2.76	2.32	4.568	4.133
		k_F	6.571	7.813	20.769	21.52
		R^2	0.996	0.986	0.905	0.999

Table 4. The comparison of adsorption capacity for MG in several adsorbents

Sorbent	Maximum Adsorption Capacity (mg/g)	References
Rattan Sawdust	62.71	[18]
MWCNTs	11.95	[44]
Leucaena leucocephala	2.389	[45]
Para-aminoBenzoic (PABA@AC)	66.87	[46]
3A-zeolite	47.17	[47]
C-ZnAl LDH	87.03	[48]
Ternary Mg/(Al+Fe)	580.50	[42]
Ds-intercalated Zn-Y hydroxides	102.98	[49]
Ni/Al LDH	27.32	[50]
Cu/Al-LDH	59.52	This work
Cu/Cr-LDH	55.86	This work

3.5. Thermodynamic study

The thermodynamic parameters, including enthalpy (ΔH), entropy (ΔS) and Gibbs energy (ΔG) was calculated in this research. The result of thermodynamic was calculated by The Van't Hoff equation, which written as followed:

$$\Delta G = -RT \ln (K_d) \quad (5)$$

$$\ln (K_d) = \frac{\Delta S}{R} - \frac{\Delta H}{RT} \quad (6)$$

with R is constant gases, and K_d is adsorption distribution coefficient. The parameters of thermodynamic determined by calculation of Van't Hoff linear regression as $1/T$ vs $\ln (K_d)$. Figure 9 shows the linearity of interaction between adsorbate and adsorbent on the effect of temperature.

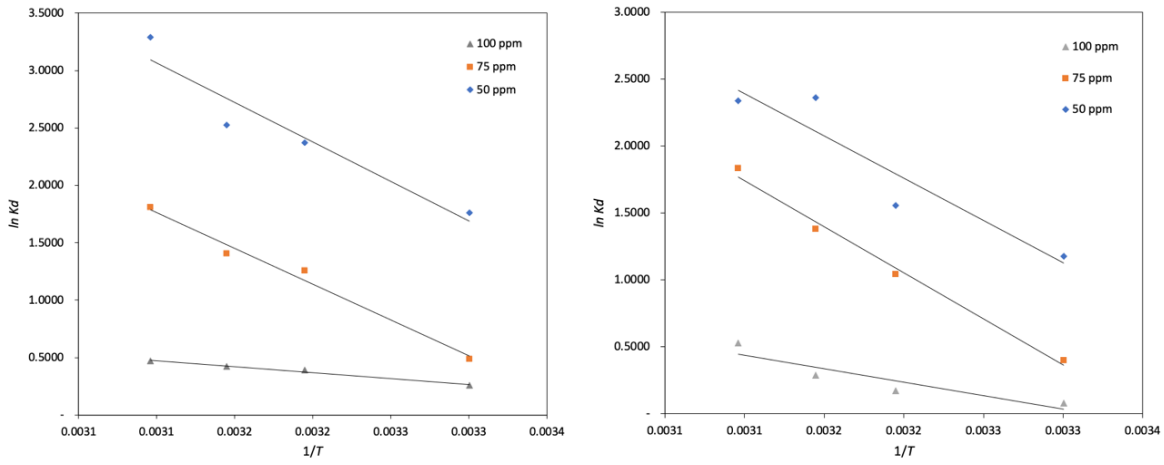

(a) **(b)**

Figure 9. Van't Hoff Plot of CuAl (a) and CuCr (b) layered double hydroxide

Gibbs energy determines the spontaneity and feasibility of the adsorption process. If the value of Gibbs energy is negative, the adsorption process occurs spontaneously. The decreases in Gibbs energy suggests the adsorption process is more spontaneous at high temperature. The positive value of entropy indicates the high affinity of the adsorbent for dye molecules. It also identified the randomness at the solid-solution interface during the adsorption process. Enthalpy value resulted from calculation confirmed that the interaction between adsorbent-adsorbate is physisorption having range 2-40 kJ/mol. The adsorption enthalpy calculated at initial concentrations of 50 mg/L indicates the adsorption process leads to chemisorption. The chemisorption process is likely to occur in low concentration with highly selective adsorbate adsorption site [51].

Table 5. Thermodynamic parameters of sorption malachite green onto Cu/Al and Cu/Cr-LDH.

T (K)	Concentration (mg/L)	Cu/Al-LDH			Cu/Cr-LDH		
		ΔG (kJ/mol)	ΔS (J/mol.K)	ΔH (kJ/mol)	ΔG (kJ/mol)	ΔS (J/mol.K)	ΔH (kJ/mol)
303	50	-2.6305	175.81	50.640	-0.9155	191.824	57.2022
313		-4.3886			-2.8337		
318		-5.2676			-3.7928		
323		-6.1467			-4.7520		
303	75	-0.8890	61.683	17.883	-0.0782	56.044	16.903
313		-1.5058			-0.6386		
318		-1.8142			-0.9189		
323		-2.1227			-1.1991		
303	100	-0.6683	30.702	8.634	-0.1950	30.07	8.916
313		-0.9753			-0.4957		
318		-1.1289			-0.6460		
323		-1.2824			-0.7964		

The adsorption process tested on both adsorbents proof that it effectively removes malachite green. Figure 10 presented the XRD pattern of samples after MG adsorption. The diffraction at 11 º and 23 º º occurred in the adsorbents adsorbing MG, suggests that adsorption process did not alter the LDH structure. The interlayer space of Cu/Al-LDH after adsorption process increases to 7.582 Å from 7.540 Å whereas, for CuCr, it decreases to 7.584 Å from initial value 7.664 Å, respectively. However, these small discrepancies indicated that MG adsorbed in interlayer does not direct perpendicularly to host layer [52].

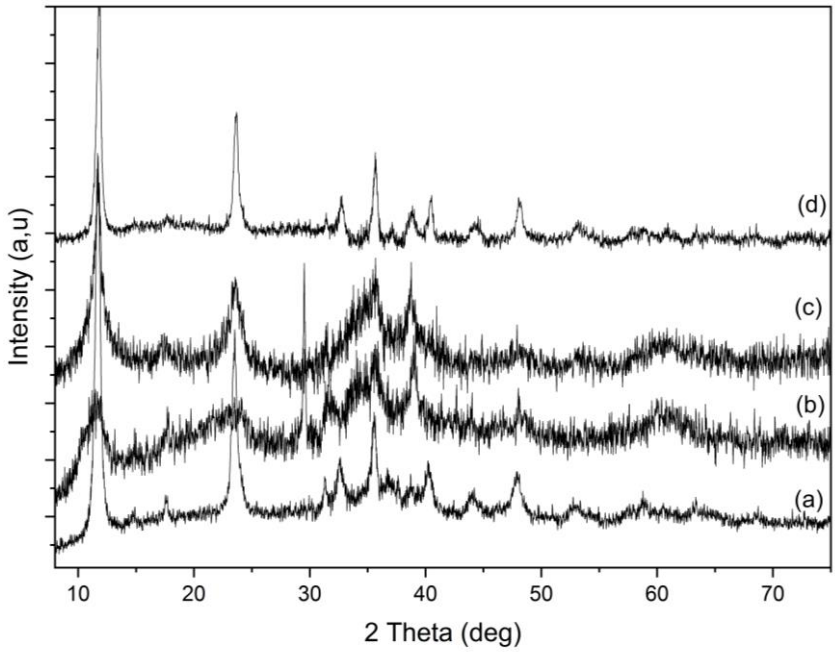

Figure 10. XRD pattern of Cu/Al (a), Cu/Cr (b), Cu/Cr-MG (c), and Cu/Al-MG (d)

3.6. Desorption Study

The desorption study was evaluated by contacting the adsorbed dye on the solid surface with water assuming that the interaction between adsorbent-adsorbate is weak. In other cases of adsorbent-adsorbate interaction, the adsorbed dye can be desorbed by using acid or alkaline water. The desorption, in this case, is driven by ion-exchange [53]. In this work, various commonly used desorption solutions were tested within the batch system in order to find the most suitable desorbing solution. The percentage of the dye desorption from the anion exchanger was calculated by:

$$\%\text{Desorption} = \frac{mass\ of\ dye\ desorbed}{mass\ of\ dye\ adsorbed}\ x\ 100\ \% \qquad (7)$$

The various solutions used in dye desorption were HCl, NaOH, NaCl, Na-EDTA, diethyl ether and $HONH_3Cl$ in the same concentration (0.01 M) (see Fig.11). The higher percent of desorption in acid solution (HCl and $HONH_3Cl$) possibly due to surface site of LDH becomes positively charged so that the electrostatic attraction of adsorbent-adsorbate and H-bonding are weakened. Furthermore, in the base condition, the desorption is also higher because of hydrophobic interaction and OH^- ions are found to have a higher affinity for the anion exchange. However, the desorption efficiency using diethyl ether, NaCl and also water shows low effectiveness on dye desorption because it desorbed less than 25% of dye adsorbed.

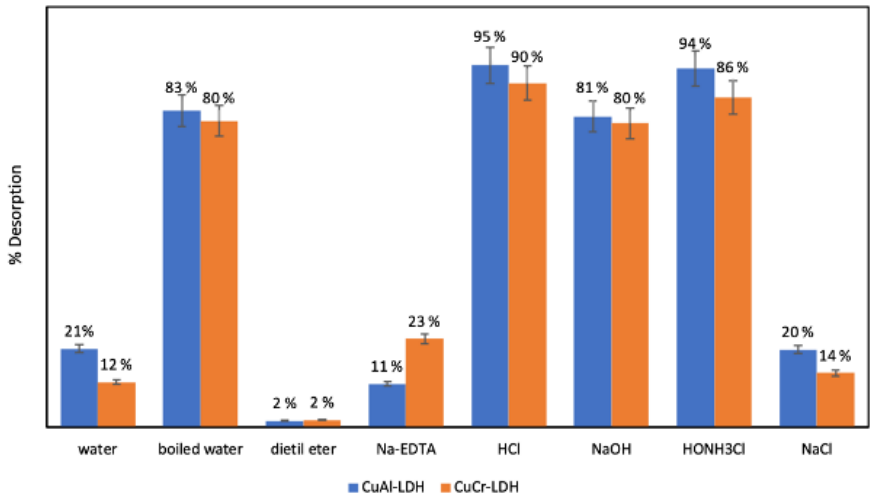

Figure 11. Malachite green desorption from CuAl and CuCr-LDHs in several solutions

3.7. Recycled adsorbent effectivity

The maximum desorption of MG from Cu/Al and Cu/Cr LDH achieved by using HCl (Fig.11), the desorption effectiveness of both LDHs are 95% and 90%. These LDHs furthermore used for regeneration purpose. The materials were washed by water for 30 minutes. The reusing cycle was conducted using ratio 0.05 g material against MG 0.05 L for two hours. The

similar procedure is repeated 3 times. Figure 12 presents the three-cycle for Cu/Al and Cu/Cr LDHs. The first cycle shows that the effectivity of both LDHs are 96% and 93%, respectively. However, the effectiveness in the adsorption of MG in the second and third cycles markedly decreased. The occurrence of structural damage after the desorption process might be responsible for this lower capacity. A similar finding was reported by Leon et al. (2018). The author concluded that when the desorption process in an acidic medium [54]; the hydrogen bonding at the interlayer was damaged. This causes the effectiveness of Cu/Al and Cu/Cr adsorption to decrease.

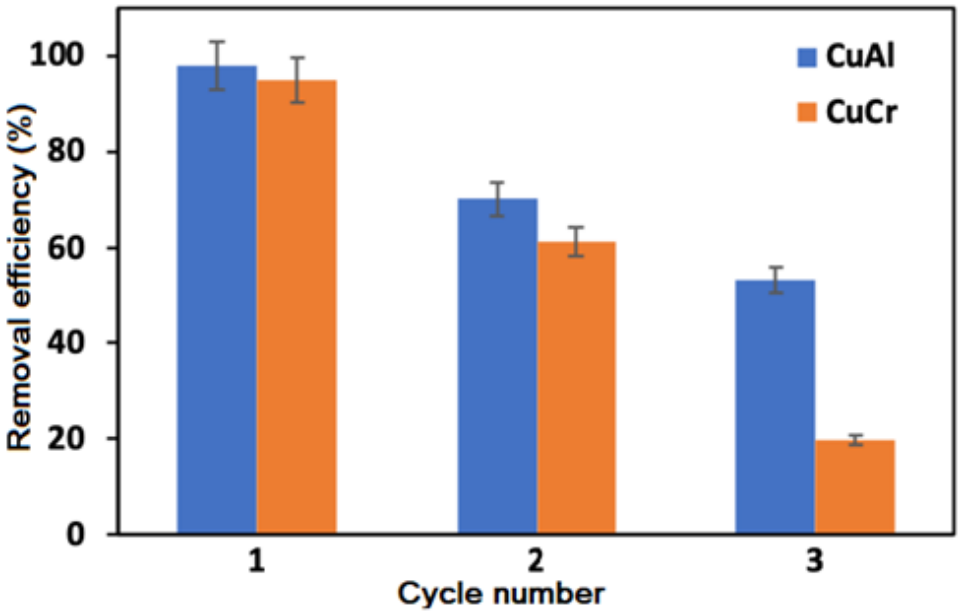

Figure 12. Regeneration study of CuAl and CuCr LDH

4. Conclusion

In the present research, Cu/Al and Cu/Cr LDHs have been used as an efficient adsorbent to remove MG from aqueous solution. The physicochemical properties of adsorbent showed that the interlayer space of Cu/Al and Cu/Cr LDHs was equivalent to surface area properties. The optimum values of pH adsorption of MG on both LDHs were achieved at pH 9. Contact time for the adsorption of MG was obtained at 70 min for Cu/Al and 120 min Cu/Cr, respectively. Findings indicate that the pseudo-second-order kinetic model showed the best-fitted with data of MG removal by both adsorbents with coefficients correlation above 0.983 for all concentrations. Isotherm study was followed Langmuir model shows the monolayer adsorption process with maximum capacity up to 59.523 mg/g. Furthermore, adsorption of MG on LDHs involves the acid-base interaction together with physical bonding between adsorbent and adsorbate.

5. Acknowledgement

The author, thanks to Universitas Sriwijaya through *Hibah Penelitian Dasar* with contract number. 0057.10/UN9/SB3.LP2M.PT/2019 in fiscal year 2019/2020.

References

1- M. T. Yagub, T.K. Sen, S. Afroze, H.M. Ang, Dye and its removal from aqueous solution by adsorption: A review, *Advances in Colloid and Interface Science*, **2014**, 209, 172–184.
2- C. Wang, A. Yediler, D. Lienert, Z. Wang, A. Kettrup, Toxicity evaluation of reactive dyestuffs, auxiliaries and selected effluents in textile finishing industry to luminescent bacteria Vibrio fischeri, *Chemosphere*, **2002**, 46, 339–344.
3- A. Kausar, M. Iqbal, A. Javed, K. Aftab, Z.H. Nazli, H.N. Bhatti, S. Nouren, Dyes adsorption using clay and modified clay: A review, *Journal of Molecular Liquids*, **2018**, 256, 395–407.
4- G. Darmograi, B. Prelot, G. Layrac, D. Tichit, G. Martin-Gassin, F. Salles, J. Zajac, Study of Adsorption and Intercalation of Orange-Type Dyes into Mg-Al Layered Double Hydroxide, *J Phys Chem C*, **2015**, 119, 23388–23397.
5- G. K. Sarma, S. Sen Gupta, K.G. Bhattacharyya, Removal of hazardous basic dyes from aqueous solution by adsorption onto kaolinite and acid-treated kaolinite: kinetics, isotherm and mechanistic study, *SN Appl Sci.*, **2019**, 1, 211.
6- Momina, M. Rafatullah, S. Ismail, A. Ahmad, Optimization Study for the Desorption of Methylene Blue Dye from Clay Based Adsorbent Coating, *Water*, **2019**, 11, 1304.
7- A. Bennani Karim, B. Mounir, M. Hachkar, M. Bakasse, A. Yaacoubi, Adsorption/desorption behavior of cationic dyes on Moroccan clay: Equilibrium and mechanism, *J. Mater. Environ.*

Sci., **2017**, 8, 1082–1096.
8- M. Oktriyanti, N.R. Palapa, R. Mohadi, A. Lesbani, Modification Of Zn-Cr Layered Double Hydroxide With Keggin Ion, *Indones. J. Environ. Manag. Sustain.*, **2019**, 3, 93–99.
9- Y. Xu, Z. Li, K. Su, T. Fan, L. Cao, Mussel-inspired modification of PPS membrane to separate and remove the dyes from the wastewater, *Chem. Eng. J.*, **2018**, 341, 371–382.
10- A.S. Kalamdhad, J. Singh, K. Dhamodharan, *Advances in Waste Management*, Springer Singapore: Singapore, **2019**. https://doi.org/10.1007/978-981-13-0215-2.
11- X. Tao, Y. Han, C. Sun, L. Huang, D. Xu, Plasma modification of NiAlCe–LDH as improved photocatalyst for organic dye wastewater degradation, *Appl. Clay Sci.*, **2019**, 172, 75–79.
12- N.R. Palapa, R. Mohadi, A. Lesbani, Adsorption of direct yellow dye from aqueous solution by Ni/Al and Zn/Al layered double hydroxides, Yogyakarta, Indonesia, **2018**. https://doi.org/10.1063/1.5064978
13- T. Taher, D. Rohendi, R. Mohadi, A. Lesbani, Thermal and Acid Activation (TAA) of bentonite as an adsorbent for removal of methylene blue: A kinetics and thermodynamic study. *Chiang Mai J. Sci.*, **2018**, 45, 1770–1781.
14- Z. Noorimotlagh, S.A. Mirzaee, S.S. Martinez, S. Alavi, M. Ahmadi, N. Jaafarzadeh, Adsorption of a textile dye in activated carbons prepared from DVD and CD wastes modified with multi-wall carbon nanotubes: Equilibrium isotherms, kinetics and thermodynamic study, *Chemical Engineering Research and Design*, **2019**, 141, 290–301.
15- R. Foroutan, R. Mohammadi, J. Razeghi, B. Ramavandi, Performance of algal activated carbon/Fe_3O_4 magnetic composite for cationic dyes removal from aqueous solutions, *Algal Research*, **2019**, 40, 101509.
16- K.-W. Jung, B.H. Choi, C.M. Dao, Y.J. Lee, J.W. Choi, K.-H. Ahn, S.-H. Lee, Aluminum carboxylate-based metal-organic frameworks for effective adsorption of anionic azo dyes from aqueous media, *Journal of Industrial and Engineering Chemistry*, **2018**, 59, 149–159.
17- U. Tezcan Un, F. Ates, Low-cost adsorbent prepared from poplar sawdust for removal of disperse orange 30 dye from aqueous solutions, *Int J Environ Sci Technol*, **2019**, 16, 899–908.
18- B.H. Hameed, M.I. El-Khaiary, Malachite green adsorption by rattan sawdust: Isotherm, kinetic and mechanism modeling, *Journal of Hazardous Materials*, **2008**, 159, 574–579.
19- O. Segun Esan, The Removal of Single and Binary Basic Dyes from Synthetic Wastewater Using Bentonite Clay Adsorbent. *Am. J. Polym. Sci. Technol.*, **2019**, 5, 16-28.
20- T. Taher, D. Rohendi, R. Mohadi, A. Lesbani, Congo red dye removal from aqueous solution by acid-activated bentonite from sarolangun: kinetic, equilibrium, and thermodynamic studies, *Arab Journal of Basic and Applied Sciences*, **2019**, 26, 125–136.
21- N.R. Palapa, B. R. Rahayu, T. Taher, A. Lesbani, R. Mohadi, Kinetic Adsorption of Direct Yellow Onto Zn/Al and Zn/Fe Layered Double Hydroxides, *sci technol indones*, **2019**, 4, 101-104.
22- Z. Yang, F. Wang, C. Zhang, G. Zeng, X. Tan, Z. Yu, Y. Zhong, H. Wang, F. Cui, Utilization of LDH-based materials as potential adsorbents and photocatalysts for the decontamination of dyes wastewater: a review, *RSC Adv*, **2016**, 6, 79415–79436.
23- M.V. Bukhtiyarova, A review on effect of synthesis conditions on the formation of layered double hydroxides, *Journal of Solid State Chemistry*, **2019**, 269, 494–506.
24- D. Tichit, G. Layrac, C. Gérardin, Synthesis of layered double hydroxides through continuous flow processes: A review, *Chemical Engineering Journal*, **2019**, 369, 302–332.
25- J. Qu, L. Sha, C. Wu, Q. Zhang, Applications of Mechanochemically Prepared Layered Double Hydroxides as Adsorbents and Catalysts: A Mini-Review, *Nanomaterials*, **2019**, 9, 80.
26- H. Zhang, H. Chen, S. Azat, Z.A. Mansurov, X. Liu, J. Wang, X. Su, R. Wu, Super adsorption capability of rhombic dodecahedral Ca-Al layered double oxides for Congo red removal, *Journal of Alloys and Compounds*, **2018**, 768, 572–581.
27- F.Z. Mahjoubi, A. Elhalil, R. Elmoubarki, M. Sadiq, A. Khalidi, O. Cherkaoui, N. Barka, Performance of Zn-, Mg- and Ni-Al layered double hydroxides in treating industrial textile wastewater, Journal of Applied Surfaces and Interfaces, **2017**, 2, 1-11.
28- S.A. Khan, S.B. Khan, A.M. Asiri, Layered double hydroxide of Cd-Al/C for the Mineralization and De-coloration of Dyes in Solar and Visible Light Exposure, *Sci Rep.*, **2016**, 6, 1-15.
29- Z. Bai, C. Hu, H. Liu, J. Qu, Selective adsorption of fluoride from drinking water using NiAl-layered metal oxide film electrode, *J. Colloid Interface Sci.*, **2019**, 539, 146–151.
30- M. Szabados, Z. Kónya, A. Kukovecz, P. Sipos, I. Pálinkó, Structural reconstruction of mechanochemically disordered CaFe-layered double hydroxide, *Appl. Clay Sci.*, **2019**, 174, 138–145.
31- X. Duan, J. Lu, D.G. Evans, Assembly Chemistry of Anion-intercalated Layered Materials, *Modern Inorganic Synthetic Chemistry*, **2011**, 375–404. https://doi.org/10.1016/B978-0-444-53599-3.10017-4.
32- X.J. Liao, G.S. Chen, A hybrid hydrogel based on clay nanoplatelets and host-guest inclusion

complexes, *Chinese Chem. Lett.*, **2016**, 27, 583–587.
33- C. Lei, M. Pi, P. Kuang, Y. Guo, F. Zhang, Organic dye removal from aqueous solutions by hierarchical calcined Ni-Fe layered double hydroxide: Isotherm, kinetic and mechanism studies, *J. Colloid Interface Sci.*, **2017**, 496, 158–166.
34- F. Amor, A. Diouri, I. Ellouzi, F. Ouanji, M. Kacimi, High efficient photocatalytic activity of Zn-Al-Ti layered double hydroxides nanocomposite, *MATEC Web Conf.*, **2018**, 149. https://doi.org/10.1051/matecconf/201814901087
35- A. Smalenskaite, L. Pavasaryte, T.C.K. Yang, A. Kareiva, Undoped and Eu^{3++} doped magnesium-aluminium layered double hydroxides: Peculiarities of intercalation of organic anions and investigation of luminescence properties, *Materials*, ***2019***, 12, 736.
36- H. Wang, G. Fan, C. Zheng, X. Xiang, F. Li, Facile sodium alginate assisted assembly of Ni-Al layered double hydroxide nanostructures, *Ind. Eng. Chem. Res.*, **2010**, 49, 2759–2767.
37- C.A. Antonyraj, P. Koilraj, S. Kannan, Synthesis of delaminated LDH: A facile two-step approach. *Chem. Commun.*, **2010**, 46, 1902.
38- S. Berner, P. Araya, J. Govan, H. Palza, Cu/Al and Cu/Cr based layered double hydroxide nanoparticles as adsorption materials for water treatment, *J. Ind. Eng. Chem.*, **2018**, 59, 134–140.
39- E.S. Zhitova, S.V. Krivovichev, I. Pekov, H.C. Greenwell, Crystal chemistry of natural layered double hydroxides. 5. Single-crystal structure refinement of hydrotalcite, $[Mg_6Al_2(OH)_{16}](CO_3)(H_2O)_4$, *Mineral. Mag.*, **2019**, 83, 269–280.
40- N. Mao, Y. Jiao, CuAl Hydrotalcite Formed CuAl-Mixed Metal Oxides for Photocatalytic Removal of Rhodamine B and Cr(VI), *ChemistrySelect*, **2018**, 3, 12676–12681.
41- K.M. Parida, L. Mohapatra, Carbonate intercalated Zn/Fe layered double hydroxide: A novel photocatalyst for the enhanced photodegradation of azo dyes, *Chem. Eng. J.*, **2012**, 179, 131–139.
42- S. Das, S.K. Dash, K.Z. Parida, Kinetics, Isotherm, and Thermodynamic Study for Ultrafast Adsorption of Azo Dye by an Efficient Sorbent: Ternary Mg/(Al + Fe) Layered Double Hydroxides, *ACS Omega*, **2018**, 3, 2532–2545.
43- S.A. Haji Azaman, A. Afandi, B.H. Hameed, A.T. Mohd Din, Removal of malachite green from aqueous phase using coconut shell activated carbon: Adsorption, desorption, and reusability studies, *J. Appl. Sci. Eng.*, **2018**, 21, 317–330.
44- Y.C. Lee, M.H.M. Amini, N.S. Sulaiman, M. Mazlan, J.G. Boon, Batch adsorption and isothermic studies of malachite green dye adsorption using leucaena leucocephala biomass as a potential adsorbent in water treatment, *Songklanakarin J. Sci. Technol.*, **2018**, 40, 563–569.
45- M. Rajabi, Adsorption of malachite green from aqueous solution by carboxylate group functionalized multi-walled carbon nanotubes: Determination of equilibrium and kinetics parameters, *J. Ind. Eng. Chem.*, **2016**, 34, 130–138.
46- F. Kovanda, Layered Double Hydroxides Intercalated With Organic Anions and. *Acta Geodyn, Geomater*, **2009**, 6, 111–119.
47- E. Sharifpour, E. Alipanahpour Dil, A. Asfaram, M. Ghaedi, A. Goudarzi, Optimizing adsorptive removal of malachite green and methyl orange dyes from simulated wastewater by Mn-doped CuO-Nanoparticles loaded on activated carbon using CCD-RSM: Mechanism, regeneration, isotherm, kinetic, and thermodynamic studies, *Appl. Organomet. Chem.*, **2019**, 33, 1–14.
48- G. George, M.P. Saravanakumar, Facile synthesis of carbon-coated layered double hydroxide and its comparative characterisation with Zn-Al LDH: application on crystal violet and malachite green dye adsorption-isotherm, kinetics and Box-Behnken design, *Environ. Sci. Pollut. Res. Int.*, **2018**, 25, 30236–30254.
49- P. Chakraborty, R. Nagarajan, Efficient adsorption of malachite green and Congo red dyes by the surfactant (DS) intercalated layered hydroxide containing Zn^{2+} and Y^{3+}-ions, *Appl. Clay Sci.*, **2015**, 118, 308–315.
50- N.R. Palapa, T. Taher, R. Mohadi, M Said, Synthesis of Ni/Al Layered Double Hydroxides (LDHs) for Adsorption of Malachite Green and Direct Yellow Dyes from Solutions : Kinetic and Thermodynamic, **2018**, 226, 020033.
51- S. Mukherjee, A. Kumar, M. Zaworotko, Metal-organic framework based carbon capture and purification technologies for a clean environment, J. *environment Republic of Ireland*, **2019**. https://doi.org/10.1016/B978-0-12-814633-0.00003-X.
52- Y. Lu, B. Jiang, L. Fang, F. Ling, J. Gao, F. Wu, X. Zhang, High-performance NiFe layered double hydroxide for methyl orange dye and Cr(VI) adsorption, *Chemosphere*, **2016**, 152, 415–422.
53- M. Greluk, Z. Hubicki, Efficient removal of Acid Orange 7 dye from water using the strongly basic anion exchange resin Amberlite IRA-958, *Desalination*, **2011**, 278, 219–226 .
54- O. León, A.M. Bonilla, D. Soto, D. Pérez, M. Rangel, M. Clina, M.F. Garcia, Removal of anionic and cationic dyes with bioadsorbent oxidized chitosans, *Carbohydr. Polym.*, **2018**, 194, 375–383.